To appear in JGR, 2002

Simulations of plasma clouds in the midlatitude *E* region ionosphere with implications for type I and type II quasiperiodic echoes

D. L. Hysell [1], M. Yamamoto, and S. Fukao

Radio Science Center for Space and Atmosphere, Kyoto University, Uji, Japan

Abstract. The electrodynamics of clouds of enhanced plasma density in the the postsunset midlatitude *E* region ionosphere are simulated in three dimensions. Such clouds become polarized in the presence of a background electric field, as would be imposed by the *F* region dynamo. If the clouds are elongated so that their major and minor axes in the horizontal plane are much larger and smaller than about 1 km, respectively, the polarization electric field can become an order of magnitude larger than the applied field. Elongated depressions or ripples in planar layers also become polarized but to a lesser degree. Electric fields and Hall drifts sufficiently large to excite Farley Buneman instabilities can be produced, particularly when neutral wind forcing is considered in addition to background electric fields. The plasma clouds are also unstable to a collisional drift instability capable of generating large-scale primary waves. A linear, local dispersion relation for this instability is derived. The primary waves are presumed to be capable of generating small-scale irregularities through mode coupling and plasma turbulence. Polarized plasma clouds drifting through the radar scattering volume may account for many of the characteristics of type I and type II quasiperiodic echoes.

1. Introduction

The discovery of quasiperiodic (QP) echoes by *Yamamoto et al.* [1991, 1992] focused renewed attention on plasma irregularities in the midlatitude *E* region. Spectrally, the preponderance of the echoes resembled the type II echoes sometimes associated with gradient drift instabilities in the equatorial electrojet, suggesting a common origin. When midlatitude type I echoes were later observed by *Haldoupis and Schlegel* [1994], *Huang and Chu* [1998], and others, interpretations rooted in Farley Buneman instabilities found in the equatorial and auroral electrojets were likewise sought [*Haldoupis et al.*, 1996; *Shalimov et al.*, 1998; *Hysell and Burcham*, 2000]. However, it was evident that the geometry and conditions found at middle latitudes are sufficiently different from those at equatorial and polar latitudes to prohibit the wholesale transplant of existing instability theories. Without the strong background currents that exist at the electrojets and without obvious routes of current closure, it is not immediately apparent how Farley Buneman instabilities can occur at middle latitudes. While sporadic *E* layers provide gradients to support gradient drift instabilities, finite parallel gradient length scale effects suppress the formation of large-scale primary gradient drift waves of the kind found at the magnetic equator [*Woodman et al.*, 1991]. Furthermore, the quasiperiodic striations characteristic of midlatitude echoes are not observed in the electrojets.

The last decade saw an explosion of QP echo theories based on generalizations of electrojet theory. Among them are theories that rely upon sporadic *E* layers deformed by gravity waves to attain appropriate geometries [*Woodman et al.*, 1991; *Tsunoda et al.*, 1994] or presuppose the existence of specific types of structures in the layers [*Haldoupis et al.*, 1996; *Shalimov et al.*, 1998; *Tsunoda*, 1998; *Maruyama et al.*, 2000], that utilize sheared winds to force gradient drift instabilities [*Kagan and Kelley*, 1998], that include finite parallel wavenumber effects [*Rosado-Roman et al.*, 1999], or that invoke thermal effects [*Kagan and Kel-*

[1] On leave from the Department of Physics and Astronomy, Clemson University, Clemson, South Carolina, USA

ley, 2000]. There appear to be many plausible theories, but which do observations favor? Parsimony argues that a simple theory that accounts for both type I and type II echoes and also for quasiperiodic striations is a strong contender.

It has been widely reported that irregular, patchy sporadic *E* layers form at middle latitudes [*Miller and Smith*, 1978; *Smith and Miller*, 1980; *Bowman*, 1989; *Maruyama*, 1991; *Maruyama et al.*, 2000]. While the source of the layers is unknown, mounting evidence suggests that neutral shear instabilities may be responsible [*Larsen*, 2000]. *Larsen* [2000] further argues that the patchy layers themselves could be the ultimate source of quasiperiodic echoes. The intent of this paper is to examine the properties of irregular or patchy plasma layers and "clouds" that become polarized by a background electric field. The importance of electrical coupling between the clouds and the *F* region by field aligned currents is stressed. We argue that the presence of such layers alone may explain the existence of both large-scale primary plasma waves, able to excite small-scale irregularities through plasma turbulence, and small-scale waves generated directly by Farley Buneman instabilities.

We revisit computational studies of polarized plasma clouds in the midlatitude *E* region ionosphere performed earlier by *Hysell and Burcham* [2000]. This time, the computations are carried out using magnetic dipole coordinates to account for the curvature of the magnetic field lines. The computations also extend much further along the flux tube into the *F* region than before. We investigate both polarized plasma clouds and ripples in planar sporadic *E* layers as sources of large electric fields and currents in the midlatitude *E* region. We confirm that polarization electric fields and Hall drifts large enough to excite Farley Buneman instabilities and give rise to type I echoes can arise in irregular, elongated sporadic *E* layers. Moreover, we study the time evolution of plasma clouds and show that they are unstable to collisional drift instabilities. Large-scale primary waves can emerge in irregular sporadic *E* layers and generate small-scale irregularities and type II echoes via plasma turbulence. Coherent echoes from small-scale irregularities in drifting clouds should then appear as striations in range-time-intensity plots.

We begin with a description of a numerical model of midlatitude *E* region irregularities. We then investigate the static response of plasma clouds with different geometries to a background electric field. The time evolution of a plasma cloud in a background field is subsequently simulated. Waves found to emerge in this simulation undergo a linear, local stability analysis. Finally, the implications for our understanding of type I and II quasiperiodic radar echoes are discussed.

2. Simulation Description

In simulating the dynamics of irregularities in the midlatitude *E* region ionosphere, we consider the low-frequency electrostatic behavior of a fluid plasma composed of electrons and multiple ions with guiding center velocities given by

$$\begin{aligned}\mathbf{v}_j &= \mu_{\perp j}\mathbf{E}_\perp + \mu_{\times j}\mathbf{E}\times\hat{b} + \mu_{\parallel j}\mathbf{E}_\parallel \\ &\quad -D_{\perp j}\nabla_\perp \ln n_j - D_{\times j}\nabla \ln n_j \times \hat{b} - D_{\parallel j}\nabla_\parallel \ln n_j\end{aligned} \tag{1}$$

where the mobilities are defined by $\mu_{\perp j} = (\nu_j/\Omega_j B)(1 + \nu_j^2/\Omega_j^2)^{-1}$, $\mu_{\times j} = (1/B)(1+\nu_j^2/\Omega_j^2)^{-1}$, and $\mu_{\parallel j} = \Omega_j/\nu_j B$ and the diffusivities by $D_{\perp j} = (\nu_j v_{tj}^2/\Omega_j^2)(1 + \nu_j^2/\Omega_j^2)^{-1}$, $D_{\times j} = (v_{tj}^2/\Omega_j)(1 + \nu_j^2/\Omega_j^2)^{-1}$, and $D_{\parallel j} = v_{tj}^2/\nu_j$. Here, $\mu_{\perp j}$ and $\mu_{\parallel j}$ are the Pedersen and parallel mobilities, and $D_{\perp j}$ and $D_{\parallel j}$ are the perpendicular and parallel diffusivities for species j. The $\mu_{\times j}$ and $D_{\times j}$ terms are the the Hall mobility and the diamagnetic drift coefficient for species j, in that order. Also, ν_j and Ω_j refer to the collision frequency and gyrofrequency of species j, respectively (see below). Note that the gyrofrequencies written above carry the sign of the charge species. The parallel and perpendicular subscripts refer to the orientation with respect to the geomagnetic field, which is parallel to $\hat{b}$. Also, v_{tj} refers to the thermal velocity $\sqrt{KT_j/m_j}$, and the other terms have their usual meaning.

Definitions of the tensor plasma conductivity Σ and diffusivity $\mathbf{D}$ follow from the contributions these drifting charge species make to the total current density in the plasma:

$$\mathbf{J} = \sum_{j+} n_j e\mathbf{v}_j - ne\mathbf{v}_e \equiv \mathbf{\Sigma}\cdot\mathbf{E} - e\mathbf{D}\cdot\nabla n \tag{2}$$

The sum in (2) is over the ion species such that $\sum_{j+} n_j = n_e = n$. The electric field and plasma number density can now be expressed in terms of background and perturbed components such that $\mathbf{E} = \mathbf{E}_\circ - \nabla\Phi$ and $n = n_\circ + \delta n$. In what follows, the perturbations Φ and δn are unknown variables to be solved for whereas the background quantities are treated as known constants.

The electrostatic potential Φ must satisfy the quasineutrality condition:

$$\nabla\cdot(\Sigma\cdot\nabla\Phi) = \nabla\cdot(\Sigma\cdot\mathbf{E}_\circ) - \nabla\cdot(e\mathbf{D}\cdot\nabla n) \tag{3}$$

which specifies the electrostatic response to an applied electric field in an inhomogeneous, anisotropic, warm plasma. This response includes the polarization and ambipolar electric fields that arise when a plasma cloud is formed. The system of equations is finally closed by the expression for ion continuity:

$$\frac{\partial n}{\partial t} + \nabla\cdot(n\mathbf{v}_i) = 0 \tag{4}$$

Here, $n\mathbf{v}_i = \sum_{j+} n_j \mathbf{v}_j$ is the total ion flux, where the plasma composition is assumed to remain constant in time but is allowed to vary with altitude.

Equation (3) represents a non-separable linear inhomogeneous elliptic partial differential equation with non-constant coefficients for the electrostatic potential Φ which can be discretized and solved numerically in three dimensions using relaxation methods. Forcing can be specified through the right side. The ion continuity equation (4), meanwhile, can be efficiently discretized and solved using finite difference methods. In practice, (3) is solved for Φ at the current timestep, (4) is solved for δn at the subsequent timestep, and the process is repeated.

The coefficient matrices involved in (3) and (4) depend on the components of the conductivity and diffusivity which depend on the ionospheric plasma concentration and composition along with the collision frequencies, themselves dependent on neutral temperature, concentration, and composition. We calculate the conductivities and diffusivities using the ion-neutral and electron-neutral and electron-ion collision frequency expressions derived by *Richmond* [1972] and *Gagnepain et al.* [1977] for a three component plasma (NO^+, O_2^+, O^+) in a three component atmosphere (N_2, O_2, O) which have been reproduced by *Forbes* [1981]. Model atmospheric and ionospheric parameters are derived from the MSIS and IRI models, respectively [*Hedin*, 1991; *Bilitza et al.*, 1993].

We solve (3) using a multigrid method like the one described by *Adams* [1991, 1989] and references therein. Multigrid methods improve upon conventional iterative schemes by computing coarse grid approximations interleaved with fine grid refinements. Large-scale features converge rapidly in the coarse grid computations while fine structure is retained in the full grid computations. Approximate solutions and corrections are transmitted between multiple grid levels by interpolation and extrapolation operators. Reviews of multigrid algorithms have been presented by *Fulton et al.* [1986], *Press et al.* [1988], and *Hackbusch and Trottenberg* [1991].

The computations are performed in magnetic dipole coordinates. This permits appropriate boundary conditions to be applied readily and also removes cross-derivative terms that would otherwise appear in the differential equations implied by (3) that would greatly slow computation. It also permits the construction of a simulation volume with a small (large) spatial extent transverse to (parallel to) the magnetic field. In this way, the effects of *F* region coupling on the development of fine structure in the *E* region may be studied. The magnetic dipole coordinates (M, L, ϕ) are defined by the transformations to polar coordinates $r/r_e = L\sin^2\theta = M/\sqrt{\cos\theta}$ in which r_e is the Earth radius and θ is the colatitude. The remaining magnetic coordinate is the longitude ϕ. Note that the Jacobian scale factors associated with magnetic dipole coordinates must be used in evaluating the spatial gradients in (3) and (4).

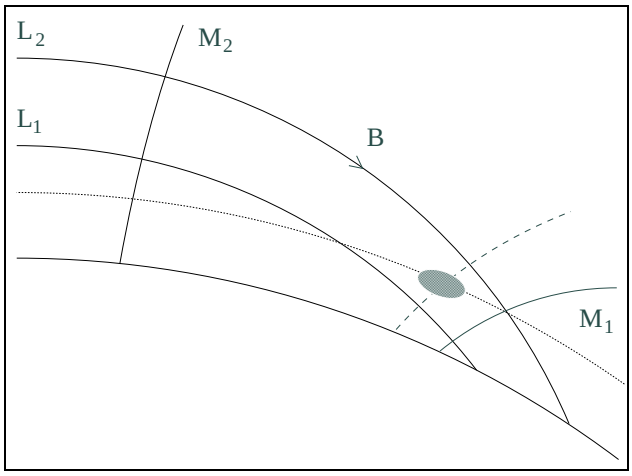

Figure 1. Representation of a cut through the 3D simulation volume at one longitude (not drawn to scale). Solid lines define the boundary of the volume in magnetic dipole coordinates. The short dashed line defines a surface of constant altitude. It passes through a cloud of enhanced plasma density pictured near the bottom of the volume. The long dashed line represents a cut through the volume on an M=constant surface. Simulation results will be plotted on such surfaces.

The solution space for the simulations is the flux tube bounded by the surfaces M_1 = 1.266, M_2 = 1.344, L_1 = 1.715, L_2 = 1.729, and $\phi = \pm 0.15°$(see Figure 1). This volume encloses the midlatitude *E* region at altitudes down to 80 km as well as the *F* region up through altitudes of 385 km. Horizontal cross-sections through the volume have dimensions of about 25 km x 25 km at *E* region altitudes. The number of grid points used to discretized the solution space along the M, L, and ϕ axes are 289, 73, and 73, respectively. This implies a spatial resolution of about 350 m (1 km) transverse to (parallel to) the magnetic field. Dirichlet boundary conditions are applied to Φ and δn on all of the boundaries. The electrostatic response to inhomogeneities associated with plasma clouds that do not extend near to the simulation boundaries is thereby presumed to vanish at the boundaries as well. Simulations are performed under conditions corresponding to 21 LT in late June, 2001 given an F10.7 solar flux level of 150 and under quiet geomagnetic conditions.

3. Static Results

Here, we present solutions to (3) corresponding to specific initial conditions imposed on δn. The background plasma density $n_\circ$ and composition are derived from the IRI model. In every case, the background electric field $\mathbf{E}_\circ$ was set to 1 mV/m southward and downward on the basis of evening climatological data from Arecibo [*Richmond et al.*, 1980]. The distributions for δn are taken to be Gaussian ellipsoids with different widths in the zonal, meridional, and vertical directions. The peak density for the ellipsoids, which are centered at an altitude of 100 km, is 2×10^5 cm^{-3}.

Figure 2 shows the results from several model runs. Each frame represents a cut through the simulation volume along a surface of constant M. The horizontal and vertical axes represent longitude and L value, respectively. Horizontal lines running through the frames indicate the altitudes intersected by the cuts in kilometers. Gray shading represents the perturbed plasma density δn along the cut. Contours denote equipotentials in volts except in the case of the lower left panel, in which case the contours denote field aligned current in μA/m^2.

The upper left panel of Figure 2 shows the electrostatic response predicted for an elongated *E* region plasma cloud with zonal, meridional, and vertical Gaussian half widths of 400 m, 5 km, and 2 km, respectively, immersed in a 1 mV/m meridional background electric field. A strong zonal polarization electric field as intense as about 6 mV/m has emerged in the main body of the cloud while electrostatic potential perturbations penetrate well outside. The equipotentials are the streamlines of the magnetized electrons which drift rapidly northward in the main body of the cloud and southward a few kilometers to the east or west of the cloud.

The polarization electric field arises to partially arrest the Hall current driven by the background meridional field which would otherwise tend to diverge in the inhomogeneous plasma cloud. However, this field also drives a strong meridional Hall current. If the *E* region plasma was electrically isolated, this Hall current would further modify the polarization electric field in such a way as to suppress both the net electric field and the current within the cloud. However, the *E* region is not isolated in this simulation but is electrically coupled to the *F* region by highly conducting magnetic field lines. Furthermore, the poles of the electric field evident in the upper left panel of Figure 2 are sufficiently distant for this electrical coupling to be efficient [*Farley*, 1959; *LaBelle*, 1985; *Hysell and Burcham*, 2000]. The strong Hall current is consequently able to close in the *F* region through field aligned currents and remain solenoidal without drastically modifying the polarization electric field.

The lower left panel of Figure 2 shows the conduction component of the field aligned current density $\sigma_\parallel E_\parallel$, where $\sigma_\parallel$ is the direct conductivity. The cut through the simulation space is made here at a larger value of M and passes well over the center of the plasma cloud midway between the *E* and *F* regions. In this panel, we find that the field aligned conduction current associated with the plasma cloud flows downward (upward) at the northern (southern) end of the cloud and approaches 1 μA/m^2 in peak intensity. The field aligned current becomes small near the top of the simulation space, indicating that most of the current has closed in the *F* region below about 385 km altitude.

The remaining four panels in Figure 2 show how plasma clouds with different geometries respond to an applied electric field. In the middle two panels, the zonal widths of the clouds are increased from the original 400 m to 1.5 and 5 km. The increase in zonal scale increases the ability of the *F* region to close the zonal Hall current driven by the background meridional electric field and effectively "short out" the entire cloud. In the rightmost two panels, the meridional widths of the plasma cloud are decreased from the original 5 km to 1.5 km and 400 m, respectively. As the meridional scale is decreased, so is the ability of the *F* region to close the meridional Hall current. The polarization electric field rotates in such a way as to arrest the current within the cloud; outside the cloud, a dipole electric field arises. Very small clouds decouple electrically from the *F* region and behave like isolated conductors and dielectrics in a background electric field.

The critical dimension which determines whether the potential structures map efficiently between the *E* and *F* region is approximately 1 km [*Farley*, 1959; *LaBelle*, 1985; *Hysell and Burcham*, 2000]. Only if a plasma cloud is elongated so that its major and minor axes are much greater than and much less than this scale, respectively, can very large polarization electric fields and strong currents arise within them. The maximum amplification of the background electric field attainable in the cloud is given by the ratio of the Hall to the Pedersen conductivity at the altitude of the cloud. This ratio is greatest at mid latitudes at an altitude of about 95 km, and the largest polarization electric fields will be generated by plasma clouds at this altitude. The actual amplification achieved depends on the cloud geometry, density, orientation, and altitude. A factor of 10 was produced in a very elongated cloud located at 97 km altitude by *Hysell and Burcham* [2000].

A variant of this principle involving a ripple irregularity in a sporadic *E* layer is illustrated in Figure 3. In this case, a broad layer with zonal, meridional, and vertical half widths of 6 km, 6 km, and 2 km, respectively is located at an altitude of 101.5 km. A depression in the layer with a maximum negative vertical displacement of 3 km has been made. The depression is also described by a Gaussian function with zonal

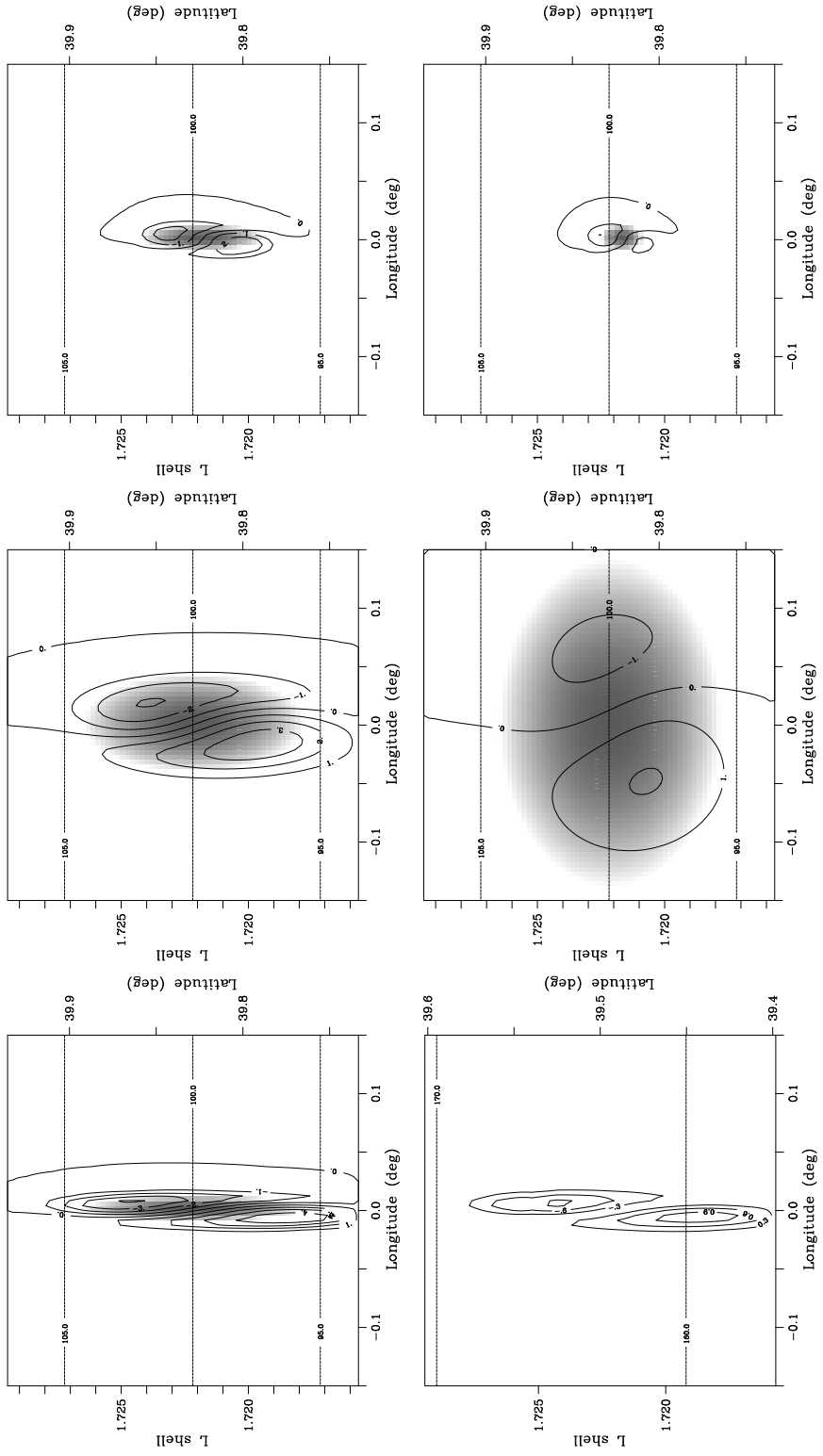

Figure 2. Simulated electrical response to plasma clouds in the midlatitude *E* region. Shaded regions represent plasma cloud densities. Contours represent equipotentials in 1 volt increments except for the plot in the lower left corner, where they denote field aligned current density in μA/m^2.

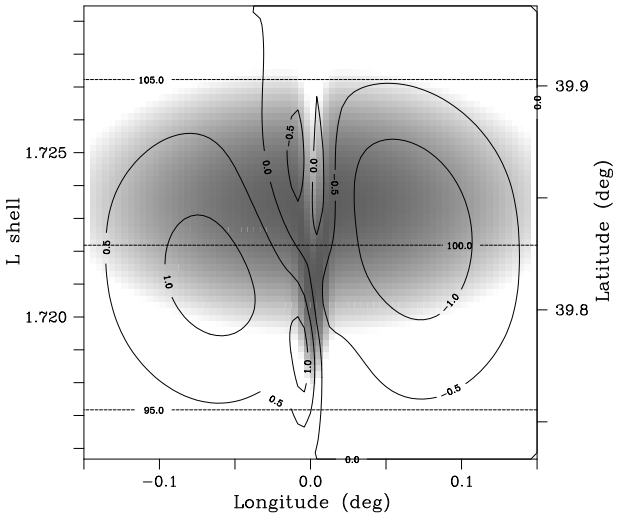

Figure 3. Simulated electrical response to a broad sporadic *E* layer with a ripple bisecting it. Contours show equipotentials in volts, and grayscales show relative electron density on a given M = constant surface.

and meridional half widths of 500 m and 5 km, respectively. Because the conductivities in the *E* region vary sharply with altitude, the depression introduces significant transverse gradients in the field line integrated conductivities much as did the plasma clouds examined above.

While the effect is less pronounced than before, Figure 3 shows that the elongated depression can lead to the generation of relatively strong polarization electric fields. The maximum electric field present here is about 1.5 mV/m, which is more intense than the background applied field. The amplification factor depends upon the layer height, thickness, and density as well as on the characteristics of the depression or ripple.

4. Time-dependent Results

Here we investigate the time evolution of *E* region plasma clouds embedded in a background electric field and coupled electrically to the *F* region ionosphere. A Gaussian ellipsoid with a peak density of 2×10^5 cm^{-3} is used to initialize δn, and the initial conditions for Φ are computed according to (3). The half-widths of the ellipsoid in the zonal, meridional, and vertical directions are 1 km, 1 km, and 2 km, respectively. The background meridional electric field is 1 mV/m. Pedersen drifts driven by this field would tend to cause the cloud to descend slowly over time. Presuming that this tendency is countered in nature by the mechanism that generates the clouds, and in order to exclude the effects of secular altitude variations on cloud evolution in the present analysis, we neglect Pedersen drifts due to $\mathbf{E}_\circ$ when evaluating (4) to keep the cloud center on station. For the time-dependent simulation, the number of grid points in the M coordinate was also reduced to 145 for computational expediency.

Figure 4 depicts the evolution of the plasma cloud over time. Initially, the tilted polarization electric field in the cloud was about 2 mV/m or about twice as intense as the background electric field. As time progresses, the cloud can be seen to expand, leading to a gradual reduction of the polarization electric field for reasons discussed in section 3. Note that transverse diffusion in the cloud is hastened by elevated potential at the cloud center, a byproduct of the parallel ambipolar electric fields in the topside and bottomside. The initial asymmetry in the equipotential lines in (10) is due to this elevation.

Eventually, longitudinal plane waves appear throughout the body of the cloud. The wavelength of the waves is about 760 m (see below), and the wavevector is approximately aligned with the initial direction of the induced polarization electric field. This alignment reflects the fact that the "seed" irregularities for the growing waves are the Fourier harmonics of the initial potential structure. The waves form first on the topside edge of the cloud in the sector where the equipotential lines are the most dense and only later appear throughout the body of the cloud. The relative amplitude of the waves approaches unity by the end of the simulation.

The perturbed density and electrostatic potential functions computed in the simulation were spectrally analyzed in three dimensions at each timestep, and it was found that the growing waveforms evident in Figure 4 were relatively narrow-banded and concentrated in a neighborhood in Fourier space centered on $k_\perp \approx 2\pi/760$ m^{-1} and with small but finite $k_\parallel$. To the extent that the waveforms are not too dispersive, the time history of a single Fourier component in this neighborhood serves as a diagnostic of their propagation and growth. Figure 5 shows the amplitude and phase of $\delta n(\mathbf{k})$ and $\Phi(\mathbf{k})$ for a dominant Fourier component versus time. The wave amplitude grew exponentially until about timestep 10, marking the end of the linear growth regime. At timestep 10, the e-folding time was about 80 s. This time can be reduced in simulations by situating the plasma cloud at higher altitude or by intensifying the forcing (see below). The wave amplitude was completely saturated by timestep 22. The period of the wave was also shortest during the linear growth regime, when it was approximately 300 s, but it increased as the wave amplitude saturated. Finally, the potential lagged the density in phase by roughly 120°–150°throughout most of the linear growth regime but by only 90°by the end of the run. The time history of this phase delay provides an important clue to the instability mechanism at work, as well as to the saturation mechanism, and will be

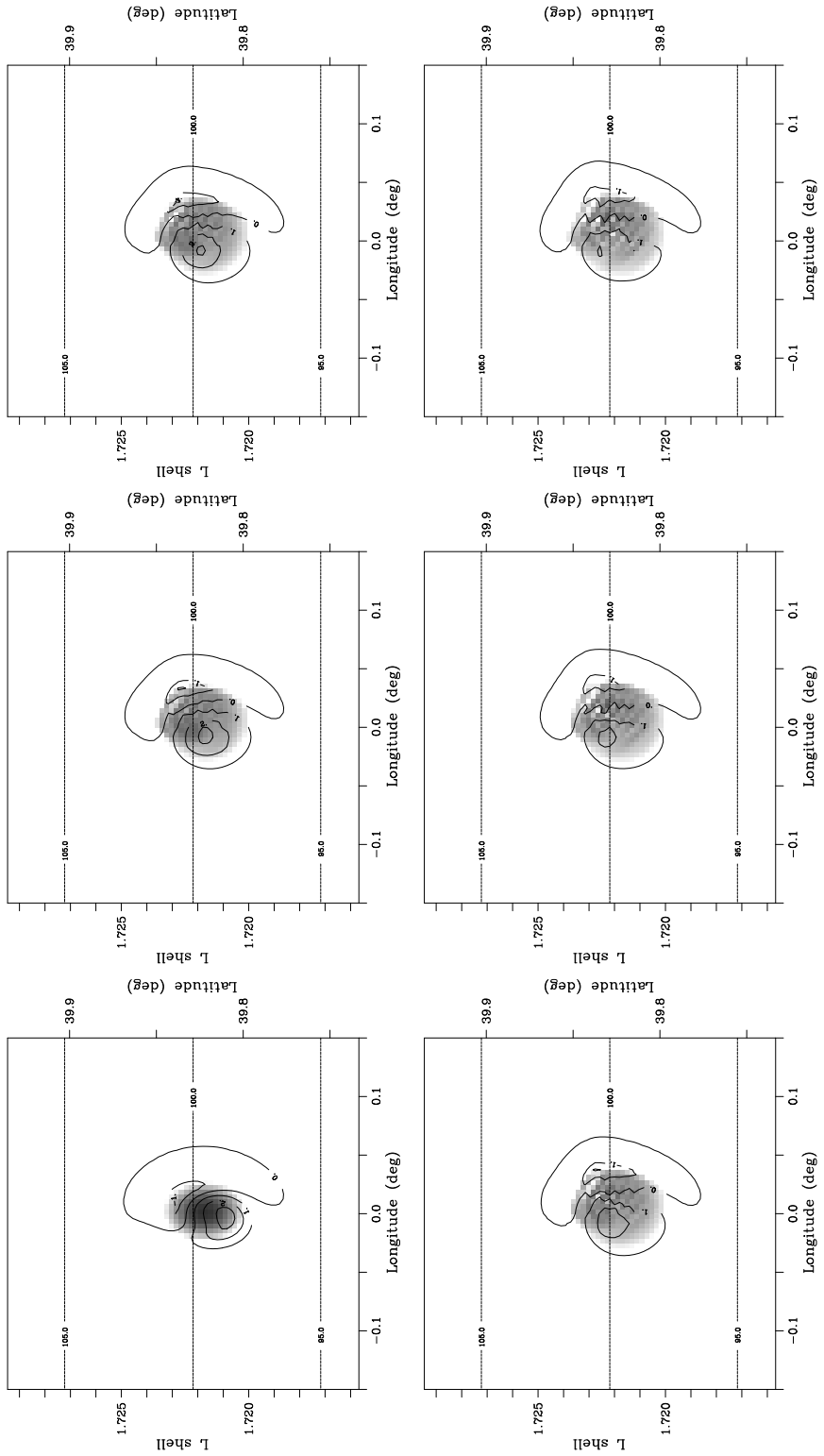

Figure 4. Time evolution of a polarized plasma cloud. Timesteps 1, 14, 16, 18, 20, and 22 are shown from left to right, top to bottom. Each timestep corresponds to 32 s elapsed time.

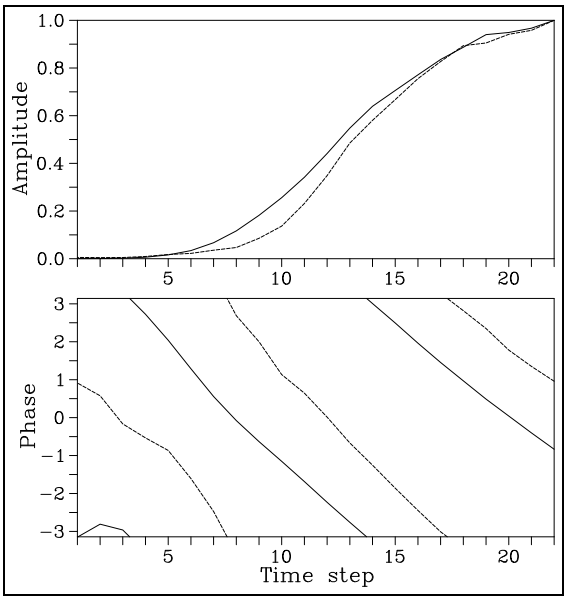

Figure 5. Diagnostics of fastest growing mode in the time-dependent simulation. Normalized wave amplitude and phase are shown in the upper and lower panels, respectively. The solid (dashed) lines correspond to the wave density (electrostatic potential). Each timestep represents 32 s of elapsed time.

shown to be indicative of finite parallel wavenumber effects.

5. Analysis

A simple linear, local dispersion relation which elucidates the most important aspects of the plasma instability found in section 4 can be derived. For the analysis, we utilize a two-dimensional Cartesian coordinate system and so neglect the effects of curved field lines along with nonlocal and nonlinear effects. The objective is to pose the simplest model possible which recovers the most important of our computational results but which is more transparent and physically illustrative. Disparities between the computational and analytic results highlight the degree to which the neglected effects are important. The linear, local dispersion relation will be shown to predict closely the behavior of the instability in its early stages and also shows that, whereas the transverse conductivity gradient length scales determine the direction and intensity of the cloud polarization, the parallel conductivity gradient length scale controls the dominant wavelength of the instability, something we can demonstrate with an additional simulation run. A more detailed, nonlocal analysis of the instability in question is planned for the future.

Consider a two-fluid plasma with electrons and ions drifting according to (1). Neglecting the diamagnetic drift terms, we can express the current density per charge as

$$\begin{aligned} \mathbf{J}/e &\approx n\mu_\perp \mathbf{E}_\perp + n\mu_\parallel \mathbf{E}_\parallel + n\mu_\times \mathbf{E}\times\hat{z} \\ &\quad -D_\perp \nabla_\perp n - D_\parallel \nabla_\parallel n \end{aligned} \tag{5}$$

where $\mu_\perp = \mu_{\perp i} - \mu_{\perp e}$, $\mu_\parallel = \mu_{\parallel i} - \mu_{\parallel e}$, $\mu_\times = \mu_{\times i} - \mu_{\times e}$, $D_\perp = D_{\perp i} - D_{\perp e}$, and $D_\parallel = D_{\parallel i} - D_{\parallel e}$, We perform a perturbation expansion in which $n = n_\circ(z) + n_1$ and $\mathbf{E} = \mathbf{E}_p + \mathbf{E}_\circ - \nabla\Phi$, where n_1 and Φ are small perturbations and where $\mathbf{E}_\circ$ and $\mathbf{E}_p$ are, respectively, the background and polarization electric fields in the cloud discussed in section 3. These fields will not in general be orthogonal. Furthermore, we assume plane wave solutions for the perturbed quantities of the form $\exp(i(k_x x + k_z z - \omega t))$, where $\omega = \omega_r + i\gamma$ is the frequency and k is the wavenumber. Here, the x and z coordinates lie in the direction of the driving polarization electric field and the magnetic field, respectively. The assumption that the growing waves propagate in the direction of the polarization electric field follows from the simulation results. Substitution of these expressions into the linearized quasineutrality condition yields a relationship between the perturbed potential and plasma number density:

$$\Phi = \frac{ik_x(\mu_\times E_\circ - \mu_\perp E_p) - D_\perp k_x^2 - D_\parallel k_z^2}{\mu_\perp k_x^2 + \mu_\parallel k_z^2 - ik_z\mu_\parallel/L}\frac{n_1}{n_\circ} \tag{6}$$

in which $E_\circ$ is the component of $\mathbf{E}_\circ$ that gives rise to a Hall current in the $\hat{x}$ direction, E_p is the total electric field in the direction of $\mathbf{E}_p$ and includes the projection of $\mathbf{E}_\circ$ in that direction, and L is a parallel conductivity gradient scale length defined by $L^{-1} = d\ln(n_\circ\mu_\parallel)/dz$. Note that both the Hall mobility and $E_\circ$ are negative quantities in a polarized plasma cloud. The term in parentheses is proportional to the horizontal current flowing across the cloud opposite the direction of propagation. This current does not vanish in a cloud which is electrically coupled to the *F* region and in which field aligned currents may flow. As was shown earlier, the width of such a cloud must exceed about 1 km. Note also that the term in which L appears influences the relative phase of the density and potential perturbations and is crucial to the instability.

The linearized ion continuity equation now reads:

$$\begin{aligned} \left(-i\omega + ik_x(\mu_{\perp i}E_p - \mu_{\times i}E_\circ) + D_{\perp i}k_x^2 + D_{\parallel i}k_z^2\right) n_1 \\ +n_\circ\mu_{\perp i}k_x^2\Phi = 0 \end{aligned} \tag{7}$$

where parallel ion conductivity has been neglected for reasons that will soon be made apparent. Wave growth depends on the Φ term in (7) having a significant real part, requiring the denominator in (6) to have a significant imaginary part. The ratio of the imaginary to the real part of the denominator is an extremum for all L when $k_z^2\mu_\parallel/k_x^2\mu_\perp = 1$. Note that

the ratio of parallel to perpendicular length scales implied by this condition is the same characteristic ratio derived by *Farley* [1959] for field aligned irregularities generally. Assuming this ratio is maintained in the present case and noting then that $k_z^2\mu_{\parallel i}/k_x^2\mu_{\perp i} \ll 1$ leads directly to the following dispersion relation:

$$-i\omega + ik_x(\mu_{\perp i}E_p - \mu_{\times i}E_\circ) + D_{\perp i}k_x^2 + D_{\parallel i}k_z^2 + \frac{\mu_{\perp i}}{\mu_\perp}\frac{ik_x(\mu_\times E_\circ - \mu_\perp E_p) - D_\perp k_x^2 - D_\parallel k_z^2}{2 - i/k_z L} = 0 \quad (8)$$

The growth rate of the waves is determined by the real part of the quotient in (8) which is now a maximum when $k_z L = 1/2$. According to (6), and in view of the fact that the term in parentheses in (6) is positive definite, this conditions implies that the potential of the fastest growing mode should lag the density in phase by 135°. The phase offsets evident in Figure 5 during the linear growth regime of the instability roughly satisfy this condition. Defining $D_{\perp a} = D_{\perp i} - D_\perp\mu_{\perp i}/4\mu_\perp$ and $D_{\parallel a} = D_{\parallel i} - D_\parallel\mu_{\perp i}/4\mu_\perp$ as the perpendicular and parallel ambipolar diffusivities for waves propagating at the assumed magnetic aspect angle, the frequency and growth rate for the fastest growing waves are then given by

$$\omega_r = \frac{1}{4}k_x\mu_{\perp i}\left(\frac{\mu_\times}{\mu_\perp}E_\circ + 3E_p\right) - k_x\mu_{\times i}E_\circ - \frac{\mu_{\perp i}}{4\mu_\perp}\left(k_x^2 D_\perp + k_z^2 D_\parallel\right) \quad (9)$$

$$\gamma = \frac{1}{4}k_x\mu_{\perp i}\left(\frac{\mu_\times}{\mu_\perp}E_\circ - E_p\right) - k_x^2 D_{\perp a} - k_z^2 D_{\parallel a} \quad (10)$$

Equation (10) states that the growth rate is proportional to the difference between the strongest polarization electric field theoretically possible in the cloud and the polarization electric field that actually emerges.

In the simulated plasma cloud, the background and polarization electric fields were about 1 mV/m and 2 mV/m, respectively. In view of the ∼30°propagation angle of the waves with respect to the meridian, however, we take $|E_\circ|$ = 0.5 mV/m and E_p = 1.13 mV/m. Furthermore, at 100 km altitude, the ratio of the Hall to the Pedersen mobility is about 14, and $\mu_{\perp i}$ is approximately 1 $\mathrm{ms}^{-1}/\mathrm{mVm}^{-1}$. Neglecting diffusive effects, the dispersion relation predicts the growth time (γ^{-1}) and period ($2\pi/\omega$) of the fastest growing wave to be 82 s and 290 s, respectively, in agreement with the simulation results in the linear growth regime. (The very close agreement is fortuitous, given the number of approximations involved.) According to (10), to the extent that the Hall current is the dominant current in the direction of wave propagation, the growth rate is proportional to $\mu_{\perp i}|\mu_\times|/\mu_\perp$. This quantity has a broad maximum between about 100 and 110 km, the range of altitudes from which the majority of QP echoes are received [*Hysell and Burcham*, 2000].

The instability in question here is like a collisional drift instability (e.g. *Cap* [1976].) When irregularities in the plasma density exist in a region with a transverse background electric field, polarization charges accumulate and polarization electric fields emerge to maintain quasineutrality. Regions of high and low electrostatic potential consequently form at the nodes of the density irregularities. If there is a finite parallel wavenumber, the regions of high and low potential are connected by common field lines and can be partly neutralized by field-aligned currents. However, as (6) shows, if there is also a background parallel conductivity gradient, the field aligned currents will alter the relative phase of the density and potential irregularities. While quasineutrality is maintained, static equilibrium is not, and plasma will converge and diverge at different phases of the wave. Wave growth and propagation result.

It might seem as though the symmetry of the plasma clouds, which have both positive and negative parallel density gradients, should stabilize them. However, the symmetry is broken by the rapid variations in collisionality with altitude. Below about 120 km altitude, the ion mobilities and diffusivities along with the parallel plasma mobility decrease rapidly with decreasing altitude. The parallel conductivity profile, which involves the product of the parallel mobility and the number density, can consequently be nearly flat in the topside of a cloud but will tend to fall off steeply in the bottomside. If this profile is either sufficiently flat or increases with altitude in the topside, the plasma cloud can be regarded as effectively having only a bottomside, characterized in the northern hemisphere by a negative value of L. This is a condition for instability and is most easily met by clouds that are not very dense or steep. In the simulation, the topside parallel conductivity profiles were flat initially only at the cloud edges where the background *E* region density made up a significant fraction of the total density, but they eventually flattened in the center of the cloud from the effects of parallel diffusion. This explains the inward progression of the instability.

The parallel plasma mobility gradient scale length is precisely -6 km at 100 km altitude and 40°latitude. The value of L in the bottomside consequently has a lower limit of -6 km for the conditions in question. In view of the preceding analysis, the fastest growing waves are therefore expected to have negative parallel wavenumbers with magnitudes no less than $|k_z| = (2|L|)^{-1} = 8.33 \times 10^{-5}\ \mathrm{m}^{-1}$. Furthermore, we have already assumed $k_x = |k_z|\sqrt{\mu_\parallel/\mu_\perp}$. Taking the radical to have a value of about 64 at 100 km altitude, we estimate that the horizontal wavelength of the fastest growing waves

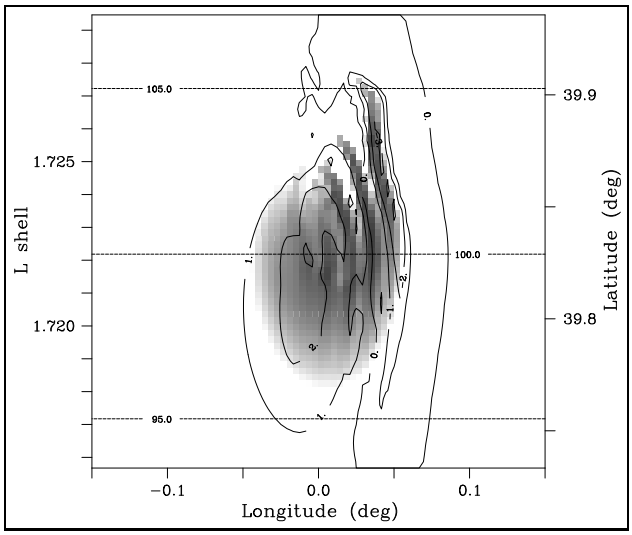

Figure 6. Results of another time dependent simulation at timestep 25. The Gaussian half-widths of the initial plasma cloud were 1.5 km, 5 km, and 2 km in the zonal, meridional, and vertical directions, respectively.

can be no more than 1180 m. In our simulation, L was closer to roughly -3 km in the regions of space that became unstable first, and the dominant wavelength was consequently closer to half this maximum wavelength. Had the wavelength been much smaller, diffusion would have damped the waves. Had the wavelength been much longer, the polarization electric fields associated with the waves would have been partially shorted out by field-aligned coupling to the *F* region.

The mechanism mainly responsible for the saturation of the instability is inaccessible to the local analysis performed here which does not rigorously treat height variations in the background parameters. Altitude variations in the coefficients on the electric field terms in (9) induce shear in the phase speeds of the growing waves. Shear in physical space acts like convection in Fourier space and causes wave energy and action to be transported in $k_\parallel$ over time. In this case, since the phase speed increases with altitude at 100 km altitude, the shift will be toward increasingly positive $k_\parallel$ in the northern hemisphere. Such a shift undermines the instability mechanism by decreasing the magnitude of $|k_z|$ and shifting the potential/density phase offset unfavorably. Note that the saturation and slowing of the wave indicated in Figure 5 coincide with the adoption of a 90°phase offset, as predicted for $k_z \approx 0$ by (6) in the nondissipative limit. In the future, we plan to perform a nonlocal analysis to better quantify the effects outlined here. On the basis of simulations, however, it appears that the waves in question are convectively stable.

Finally, Figure 6 shows the late-time behavior of another simulation run. This one was performed under the same conditions as the last except that the cloud has been widened in the zonal and meridional directions. The magnitude of the driving polarization electric field that arises in the cloud is still about 2 mV/m but is now directed nearly eastward because of the elongated cloud geometry. Also, the background meridional electric field term is included in the evaluation of (4) here, and the cloud now descends slowly over time as a result, suppressing the formation of irregularities on the bottomside. Most importantly, the parallel density gradient length scale is increased by the new cloud dimensions. Consequently, so is the wavelength of the fastest growing unstable wave, something which is immediately obvious from Figure 6. The wavelength of the dominant mode here is about 1150 m, essentially the theoretical maximum. Note that the electric field in the immediate vicinity of some of the emergent waveforms is very intense for reasons that were discussed in section 3. This simulation shows that waveforms with wavelengths of the order of a kilometer can be unstable and that the emergent waveforms themselves, being highly elongated, can become very strongly polarized. This may explain how such very elongated features come into being in nature in the first place.

6. Evaluation and summary

We have investigated the static and time-dependent behavior of polarized plasma clouds and irregularities in midlatitude sporadic *E* layers in an effort to understand the source of the small-scale irregularities detected there by coherent scatter radars. It has been shown that polarization electric fields an order of magnitude more intense than the background applied field can arise in very elongated layer structures with minor axes less than about 1 km and that these fields can drive strong Hall currents able to close in the *F* region. Furthermore, irregular or patchy sporadic *E* layers appear to be unstable to large-scale collisional drift instabilities. The growth rate is proportional to the electric fields in the layer, and the dominant wavelength is likely to be approximately 1 km or less. Electrical coupling to the *F* region is necessary for instability.

In all the analyses presented above, forcing was supplied by a 1 mV/m background southward electric field. However, neutral winds provide another important source of forcing. We may regard the simulations presented above as having been carried out in the neutral frame of reference and reinterpret the electric field in that frame as $\mathbf{E}' = \mathbf{E} + \mathbf{u} \times \mathbf{B}$, where $\mathbf{u}$ is the neutral wind velocity. A 100 m/s westward wind is equivalent to a 5 mV/m southward electric field with regard to its ability to polarize, drive Hall currents, and excite instabilities within an *E* region plasma cloud. Wind speeds of

the order of 100–150 m/s appear to be commonplace in the lower thermosphere after sunset [*Larsen*, 2002].

Obtaining polarization electric fields and Hall drifts large enough to excite Farley Buneman instabilities and give rise to type I echoes in irregular sporadic *E* layers found in nature consequently seems to pose no fundamental theoretical problems. Nor does exciting large-scale primary waves with growth times of the order of a few minutes. We presume that the large-scale primary waves are able to generate the small-scale irregularities responsible for coherent backscatter and type II echoes by means of plasma turbulence in a manner analogous to that described by *Sudan* [1983], although our simulation lacks the resolution necessary to verify this. Coherent scatter from irregularities embedded in sporadic *E* layer patches and clouds drifting toward or away from the radar would appear as striations in range-time-intensity diagrams. In a companion paper, we argue that imaging radar data support this hypothesis and also that quasiperiodicity results when there are multiple clouds in the radar antenna beam.

Note that the plasma layers and clouds investigated above were composed of atomic and molecular ions for expediency. In nature, the instabilities studies here would be strongly damped by recombination unless the layers in question were composed of metallic ions. We assume that the sporadic *E* layers and irregularities that underlie quasiperiodic echoes are, in fact, composed of metallic ions and therefore regard the time-dependent simulations presented in section 4, which incorporated atomic and diatomic ions, as illustrative approximations of the natural processes. Metallic clouds should behave in a similar way except that they would diffuse and recombine more slowly.

The source of irregular and patchy sporadic *E* layers at mid latitudes is not understood, although there is mounting evidence that neutral shear instabilities are responsible [*Larsen*, 2000]. Moreover, it is not known whether the waves simulated here would grow to dominate the intermediate-scale gradient drift waves predicted by *Rosado-Roman et al.* [1999] or vise versa. Evidence that kilometer-scale waves are dominant in midlatitude *E* region plasma clouds was provided by *Kelley et al.* [1995] who probed a thick, dense cloud suspended over a sharp sporadic *E* layer with a sounding rocket in a volume in which what appear in retrospect to have been quasiperiodic echoes were detected. Data from their rocket, which reached apogee just below 120 km and which moved nearly horizontally through the cloud, revealed the presence of large-amplitude, monochromatic, kilometric plasma density waves. A spectrum of secondary gradient drift waves also appeared to be present. Further evidence of kilometric waves in patchy sporadic *E* layers of this kind, supported by simultaneous observations of QP echoes and coupled with information about the neutral flow in the vicinity of the layers, could lead to a complete picture of the phenomenon.

Acknowledgments. This work was supported by the National Science Foundation through NSF grant ATM-0080338 to Clemson University. The MUDPACK package used for this research (copyright John C. Adams) was obtained from the University Corporation for Atmospheric Research which is sponsored by the National Science Foundation. DLH was supported by RASC as a visiting associate professor during the preparation of this manuscript.

References

Adams, J., MUDPACK: Multigrid fortran software for the efficient solution of linear elliptic partial differential equations, *Applied Math. and Comput.*, *34*, 113, 1989.

Adams, J., Multigrid software for elliptic partial differential equations: MUDPACK, *Tech. rep.*, NCAR Technical Note-357+STR, 1991.

Bilitza, D., K. Rawer, L. Bossy, and T. Gulyaeva, International Reference Ionosphere: - Past, present, future, *Adv. Space Res.*, *13, #3*, 3, 1993.

Bowman, G. G., Quasi-periodic scintillations at mid-latitudes and their possible association with ionospheric sporadic-*E* structures, *Ann. Geophys.*, *7*, 259, 1989.

Cap, F. F., *Handbook of Plasma Instabilities*, vol. 1, Academic, New York, 1976.

Farley, D. T., A theory of electrostatic fields in a horizontally stratified ionosphere subject to a vertical magnetic field, *J. Geophys. Res.*, *64*, 1225, 1959.

Forbes, J. M., The equatorial electrojet, *Rev. Geophys.*, *19*, 469, 1981.

Fulton, S., R. Ciesielski, , and W. Schubert, Multigrid methods for elliptic problems: a review, *Monthly Weather Review*, *114*, 943, 1986.

Gagnepain, J., M. Crochet, and A. D. Richmond, Comparison of equatorial electrojet models, *J. Atmos. Terr. Phys.*, *39*, 1119, 1977.

Hackbusch, W., and U. Trottenberg, *Multigrid Methods III*, Birkhauser, Boston, 1991.

Haldoupis, C., and K. Schlegel, Observation of the modified two-stream plasma instability in the midlatitude *E* region ionosphere, *J. Geophys. Res.*, *99*, 6219, 1994.

Haldoupis, C., K. Schlegel, and D. T. Farley, An explanation for type 1 radar echoes from the midlatitude *E*-region ionosphere, *Geophys. Res. Lett.*, *23*, 97, 1996.

Hedin, A. E., Extension of the MSIS theromspheric model into the lower and middle atmosphere, *J. Geophys. Res.*, *96*, 1159, 1991.

Huang, C. M., and Y. H. Chu, First observations of type-1 sporadic *E* irregularities in the equatorial anomaly region using the Chung-Li VHF radar, *Geophys. Res. Lett.*, *25*, 3779, 1998.

Hysell, D. L., and J. Burcham, The 30 MHz radar interferometer studies of midlatitude *E* region irregularities, *J. Geophys. Res.*, *105*, 12,797, 2000.

Kagan, L. M., and M. C. Kelley, A wind-driven gradient drift mechanism for midlatitude *E*-region ionospheric irregularities, *Geophys. Res. Lett.*, *25*, 4141, 1998.

Kagan, L. M., and M. C. Kelley, A thermal mechanism for generation of small-scale irregularities in the ionospheric *E*-region, *J. Geophys. Res.*, *105*, 5291, 2000.

Kelley, M. C., D. Riggin, R. F. Pfaff, W. E. Swartz, J. F. Providakes, and C. S. Huang, Large amplitude quasi-periodic fluctuations associated with a midlatitude sporadic *E* layer, *J. Atmos. Terr. Phys.*, *57*, 1165, 1995.

LaBelle, J., Ionospheric turbulence: Case studies in equatorial spread *F* and development of a rocket-borne interferometer, Ph.D. thesis, Cornell University, Ithaca, NY, 1985.

Larsen, M. F., A shear instability seeding mechanism for quasi-periodic radar echoes, *J. Geophys. Res.*, *105*, 24,931, 2000.

Larsen, M. F., Winds and shears in the mesosphere and lower thermosphere: results from four decades of chemical release wind measurements, *J. Geophys. Res.*, 2002, in press.

Maruyama, T., Observations of quasi-periodic scintillations and their possible relation to the dynamics of *E*s plasma blobs, *Radio Sci.*, *26*, 691, 1991.

Maruyama, T., S. Fukao, and M. Yamamoto, A possible mechanism for echo-striation generation of radar backscatter from midlatitude sporadic *E*, *Radio Sci.*, *35*, 1155, 2000.

Miller, K. L., and L. G. Smith, Incoherent scatter radar observations of irregular structure in mid-latitude sporadic *E* layers, *J. Geophys. Res.*, *83*, 3761, 1978.

Press, W. H., B. P. Flannery, S. A. Teukolsky, and W. T. Vetterling, *Numerical Recipes in C*, Cambridge Univ. Press, New York, 1988.

Richmond, A. D., Numerical model of the equatorial electrojet, *Tech. Rep. AFCRL-72-0668, ERP 421*, Air Force Cambridge Research Lab., Hanscom AFB, Bedford, MA, 1972.

Richmond, A. D., et al., An empirical model of quiet-day ionospheric electric fields at middle and low latitudes, *J. Geophys. Res.*, *85*, 4658, 1980.

Rosado-Roman, J. M., W. E. Swartz, and D. T. Farley, Radar studies in Puerto Rico of mid-latitude *E*-region plasma instabilities, paper presented at the XXVI URSI General Assembly, Toronto, Canada, August 13-21, 1999.

Shalimov, S., C. Haldoupis, and K. Schlegel, Large polarization electric fields associated with midlatitude sporadic *E*, *J. Geophys. Res.*, *103*, 11,617, 1998.

Smith, L. G., and K. L. Miller, Sporadic- layers and unstable wind shears, *J. Atmos. Terr. Phys.*, *42*, 45, 1980.

Sudan, R. N., Unified theory of type I and type II irregularities in the equatorial electrojet, *J. Geophys. Res.*, *88*, 4853, 1983.

Tsunoda, R. T., On polarized frontal structures, type-1 and quasiperiodic echoes in midlatitude sporadic *E*, *Geophys. Res. Lett.*, *25*, 2641, 1998.

Tsunoda, R. T., S. Fukao, and M. Yamamoto, On the origin of quasi-periodic backscatter from sporadic *E*, *Radio Sci.*, *29*, 349, 1994.

Woodman, R. F., M. Yamamoto, and S. Fukao, Gravity wave modulation of gradient drift instabilities in mid-latitude sporadic *E* irregularities, *Geophys. Res. Lett.*, *18*, 1197, 1991.

Yamamoto, M., S. Fukao, R. F. Woodman, T. Ogawa, T. Tsuda, and K. Kato, Mid-latitude *E* region field-aligned irregularities observed with the MU radar, *J. Geophys. Res.*, *96*, 15,943, 1991.

Yamamoto, M., S. Fukao, T. Ogawa, T. Tsuda, and S. Kato, A morphological study of mid-latitude *E*-region field-aligned irregularities observed with the MU radar, *J. Atmos. Terr. Phys.*, *54*, 769, 1992.

Received X; revised X; accepted X.